ASTRONOMY & ASTROPHYSICS
SUPPLEMENT SERIES

Astron. Astrophys. Suppl. Ser. **113,** 91-106 (1995)

Interesting lines in the infrared solar spectrum. III. A polarimetric survey between 1.05 and 2.50 μm

I. Rüedi[1], S.K. Solanki[1], W. Livingston[2] and J. Harvey[2]

[1] Institute of Astronomy, ETH–Zentrum, CH–8092 Zürich, Switzerland
[2] National Solar Observatory, NOAO*, P.O. Box 26732, Tucson, AZ 85726, U.S.A.

Received December 14, 1994; accepted February 25, 1995

Abstract. — We present a survey of Stokes I, V and Q in the near infrared spectral range between 1.05 and 2.50 μm, based on Fourier transform spectrometer data obtained in a sunspot umbra and in an active region plage. We discuss the diagnostic potential of a number of lines for studying solar magnetic features. These include the Ti I multiplet near 22000 Å, the Fe I $g = 3$ line at 15648.5 Å, He I 10830 Å, high excitation C I lines, as well as CO and CN lines. As an example, we provide the first estimate of the field strength gradient averaged over the height range covered by the photosphere and chromosphere. We also identify lines that show large Stokes V or Q amplitudes and analyze their profile asymmetries. In our J-band plage spectrum the Stokes V and Q profiles show an extremely large blue-red asymmetry, whose origin is not yet clear. As an incidental result we obtain the first measured value of the vertical gradient of the magnetic field strength in a plage. Averaged over approximately 1500−2000 km it corresponds to roughly 0.6 G km^{-1}.

Key words: line: identification — line: profiles — Sun: faculae, plages — Sun: infrared — Sun: magnetic fields — polarization — sunspots

1. Introduction

The wavelength dependence of the Zeeman effect accords to the infrared a unique potential for the measurement of magnetic fields in the solar atmosphere. A part of this potential has already been fulfilled (see the reviews by Deming et al. 1994; Rabin 1994; Solanki 1994; Steiner 1994 and the recent papers by Solanki et al. 1993, 1994b; Hewagama et al. 1993; Bruls et al. 1995; Bruls & Solanki 1995; Balthasar & Schmidt 1994), but much of it remains untapped. The maximum benefit can be derived from this spectral range only if a list of lines having particularly useful properties (large Landé factor, strong Stokes V or Q amplitude, etc.) is available. A number of spectral atlases of the infrared exist (e.g. Hall 1974; Delbouille et al. 1981; Farmer & Norton 1989; Livingston & Wallace 1991; Wallace & Livingston 1992; Wallace et al. 1993, 1994) and Papers I and II of the present series (Solanki et al. 1990; Ramsauer et al. 1995) provide identifications and magnetic parameters, such as the effective Landé factor $g_{\rm eff}$, of unblended lines between 1 and 2 μm. However, only in Paper I has polarimetric information been used to select lines useful for the investigation of solar magnetism: it lists lines in the infrared H-band, i.e. 1.49 − 1.8 μm recorded in a network area with strong Stokes V amplitudes. In the present work, we consider a larger wavelength range, namely 1.03 − 2.81 μm, [i.e. covering the photometric J (centered on 1.25 μm), H (centered on 1.65 μm) and K (centered on 2.2 μm) bands], analyze observations of Stokes Q in addition to Stokes V and investigate spectra obtained in both plage and a sunspot umbra. We pay particular attention to the following points:

1. The identification of lines exhibiting large Stokes V amplitudes. Such lines provide a good signal to noise ratio for accurate measurements of the magnetic splitting, the analysis of the profile shapes or magnetogram type observations.
2. Selection of spectral lines having particularly interesting properties, such as very low or high formation heights, large Landé factors, etc. We also develop simple methods for the analysis of some of these lines.
3. The search for lines showing strong Stokes Q signals, which should allow the magnetic vector to be better constrained.

* Operated by the Association of Universities for Research in Astronomy, Inc. (AURA) under cooperative agreement with the National Science Foundation

Table 1. Observations

Date	Starting time	Region	λ–range [μm]	μ	Observed Stokes profiles	Integration time [min]	Resolving power	Starting airmass	Ending airmass
30 Jan 1991	09:14	Plage	1.03–1.48	0.65	IVQ	58	400 000	2.88	2.05
30 Jan 1991	13:51	Plage	1.39–2.01	0.70	IVQ	44	300 000	1.63	1.82
31 Jan 1991	11:37	Plage	1.97–2.81	0.47	IV	46	300 000	1.60	1.53
30 Jan 1991	11:56	Umbra	1.03–1.48	0.52	IVQ	52	400 000	1.57	1.54
30 Jan 1991	15:00	Umbra	1.39–2.01	0.47	IVQ	21	300 000	1.98	2.18
31 Jan 1991	12:30	Umbra	1.97–2.81	0.43	IV	38	300 000	1.53	1.54

4. Identification of lines showing peculiar Stokes V and/or Stokes Q asymmetries, which, in some cases, are much stronger than those generally observed in the optical.

2. Observations

The observations were made on 30–31 January 1991 with the McMath-Pierce solar telescope on Kitt Peak and the 1-m Fourier transform spectrometer (FTS) extended to function as a polarimeter. The observing procedure was very similar to that described in detail by Stenflo et al. (1987a, b). The data consist of 6 spectra, 3 originating from plages and 3 from the darkest part of a sunspot umbra (member of group NOAA 6469). The Stokes parameters I (intensity) and V (the difference between right and left circularly polarized light) were measured for all of them. Stokes Q (the difference between two orthogonal linear polarizations) was also recorded except for the two scans between 1.97 and 2.81 μm. The data are summarized in Table 1. The location of the observations on the solar disk is indicated by $\mu = \cos\theta$, where θ is the heliocentric angle. The circular entrance aperture to the FTS had a diameter corresponding to 5″ for all the spectra. The effectively analyzable λ-range is restricted to 1.05 μm (by noise) to 2.5 μm (by telluric absorption).

Due to the different times at which the spectra were observed, it was not possible to ensure exact spatial coalignment of the spectra of a given type of feature (e.g. due to evolution of the magnetic features), although this was attempted for the 3 umbral spectra. Consequently the field strengths, filling factors and thermal structures of the solar features underlying the different wavelength ranges need not be the same, which must be kept in mind when comparing the results of one spectral band with another.[1] We have surveyed the data in two ways, first we have picked out a number of lines which we considered to be interesting for one reason or another. Then, in a next step we have systematically searched for lines showing particular properties, e.g. large Stokes V or Q amplitudes, large Stokes V asymmetry, etc. We begin with a discussion of individual lines.

3. The Fe I 15648 Å line

The Fe I 15648 Å line, a normal Zeeman triplet, with a large Landé factor ($g = 3$) has already proved to be a very important diagnostic for magnetic field strength measurements in plages (e.g. Harvey & Hall 1975; Zayer et al. 1989; Rabin 1992a, b; Rüedi et al. 1992) as well as in sunspots (Kopp & Rabin 1992; McPherson et al. 1992; Solanki et al. 1992b). The diagnostic properties of this line have been discussed in detail by Solanki et al. (1992a) and we only give a brief summary here.

Due to its large Landé factor, the Stokes V profile of this line is already completely split at 300–400 G in a height-independent magnetic field. Larger field strengths are simply proportional to the wavelength difference between its σ-component peaks. It is formed in the deep photosphere ($\log\tau_{1.6} \lesssim -1$) and is only moderately temperature sensitive. In umbrae, molecular and atomic lines blend its Stokes I profile. The other Stokes parameters are also affected by these blends, although to a lesser extent. The Stokes I, V and Q profiles of this line in the observed umbra are plotted in Figs. 1a–c. The distortion of the Stokes V profile due to the blending lines manifests itself close to line center, as well as in the asymmetry between the width and amplitude of the two σ-components (the blue wing is 20% broader than the red wing, but has an approximately 15% lower amplitude). The Stokes I profile shows the opposite behaviour, namely deeper and slightly narrower blue wing than red wing. The σ-components of the Stokes Q profile (Fig. 1c) are also unequal. These blends reduce the accuracy of the measured field strength in umbrae, as do the increasingly prominent damping wings at lower temperatures (see Solanki et al. 1992a and Fig. 1b). In umbrae cooler than the one considered here both the blends and the wings pose larger problems. Another diagnostic line less affected by blends and saturation at low temperatures would be very

[1] We had originally hoped to calibrate the Stokes V and Q scales of all wavelength ranges to a common value in order to account for these possible filling factor variations, but this could unfortunately not be achieved due to the absence of lines with sufficiently large Stokes V amplitude in the overlapping wavelength range. The reduced predispersor throughput at the edge of the selected wavelength range, as well as the strong atmospheric absorption at the wavelengths of overlap, are the main culprits.

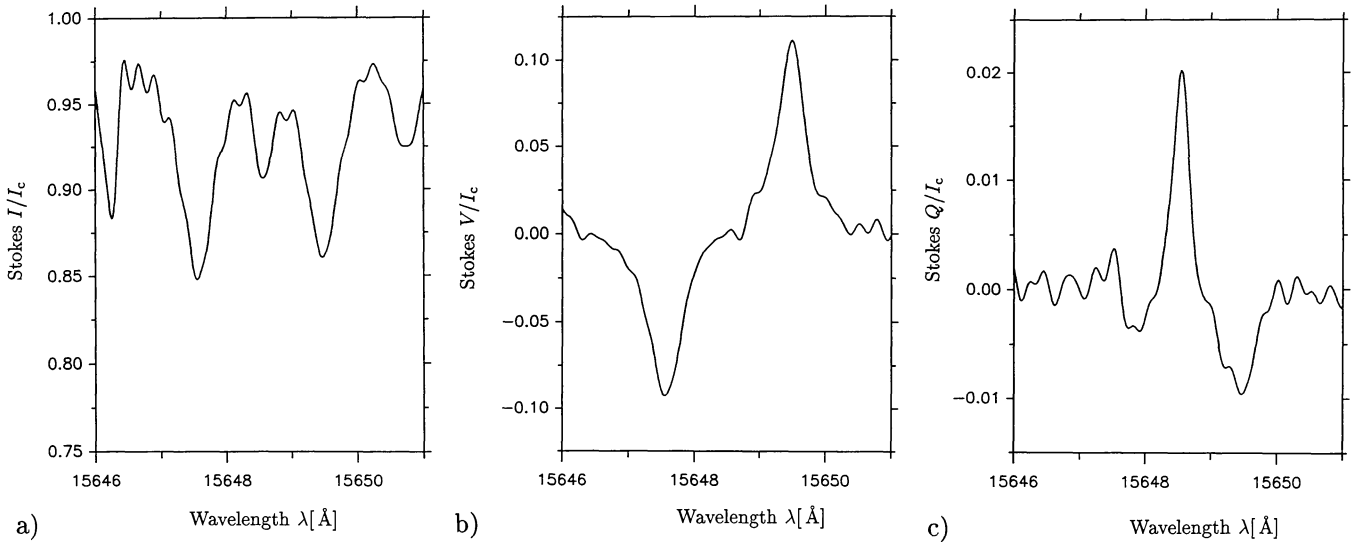

Fig. 1. Observed umbral Stokes profiles of Fe I 15648.5 Å (Landé $g = 3$) a) Stokes I, b) Stokes V, c) Stokes Q

convenient for more precise measurements of umbral fields. Such a line is discussed in Sect. 4.

One of the advantages of the large Zeeman sensitivity of the 15648 Å line is that when used in combination with an otherwise similar line having a smaller $g_{\rm eff}$ (usually Fe I 15653 Å with $g_{\rm eff} = 1.53$ has been used due to its spectral proximity) magnetic field strength gradients and distributions and the turbulence velocity can be determined (cf. Zayer et al. 1989). Due to the blending problem this diagnostic property is severely curtailed in dark umbrae. In spite of the above caveats we have determined the field strength from the plotted Stokes I and V profiles. They give $B = 2710$ G (Stokes I) and 2830 G (Stokes V).

4. The titanium multiplet at 2.2 μm

Low excitation lines of Ti I are very sensitive to temperature over the range found in the photosphere, partly due to the relatively low ionization potential of neutral Ti (6.82 eV) and partly the low Ti abundance relative to Fe (4.7 for Ti vs. 7.5 for Fe on a logarithmic scale on which hydrogen has abundance 12), which reduces the strength of Ti lines and causes even allowed transitions, like the ones we are about to discuss, to be unsaturated (saturated lines are generally less temperature sensitive). The Ti I multiplet we consider here has previously been employed by Saar & Linsky (1985) and Linsky & Saar (1987) to measure magnetic fields on active M dwarfs. The multiplet consists of 5 lines, all of which practically disappear in the spectrum of the quiet sun, but are quite prominent in umbral spectra. The wavelengths, transitions and effective Landé factors of these lines are listed in Table 2. The first line in the list, a Zeeman triplet with $g = 2.5$, turns out to complement the Fe I 15648 Å line ideally. Whereas the Fe line provides the most accurate field strengths outside umbrae, the Ti I lines only come into their own within umbrae, though they are still present in the quiet sun with depths relative to the continuum level of 2% or less (Livingston & Wallace 1991).

Table 2. Titanium multiplet

Ion	λ [Å]	Transition	$g_{\rm eff}$	$\chi_{\rm e}$ [eV]
Ti I	22310.61	$a\ ^5P_1 - z\ ^5D^\circ_0$	2.500	1.73
Ti I	22274.07	$a\ ^5P_3 - z\ ^5D^\circ_3$	1.583	1.75
Ti I	22232.91	$a\ ^5P_2 - z\ ^5D^\circ_2$	1.667	1.74
Ti I	22211.22	$a\ ^5P_1 - z\ ^5D^\circ_1$	2.000	1.73
Ti I	21897.38	$a\ ^5P_2 - z\ ^5D^\circ_3$	1.167	1.74

Figure 2b shows an umbral Stokes V profile of the first line, a Zeeman triplet at 22310 Å. Note how different this profile is from the one shown in Fig. 1b, although both give almost exactly the same field strength ($B = 2820$ G from the Stokes V profile of the Ti I line). The $g\lambda$ value, which is often taken as a measure of Zeeman separation, of the Ti I line is only marginally larger than that of the Fe I 15648 Å. Nevertheless the σ-components of the Ti I line are clearly much better separated than the σ-components of the Fe I line. This is a result of the smaller relative half-width and the absence of damping wings in the Ti I line (it is practically unsaturated, while the Fe I line already shows considerable signs of saturation in the umbra). Since the σ-half-widths of Ti I and Fe I lines are similar on a wavelength scale, the fact that $\Delta\lambda_{\rm H} \sim g\lambda^2$ means that the peak separation is a factor of 1.7 better for the Ti I line.

The Stokes V profile of this line, if considered on its own, might suggest that it is relatively unblended. This is patently not the case, as a glance at the corresponding Stokes I profile (Fig. 2a) shows. The strong blend in the middle, a telluric methane line, makes this spectrum

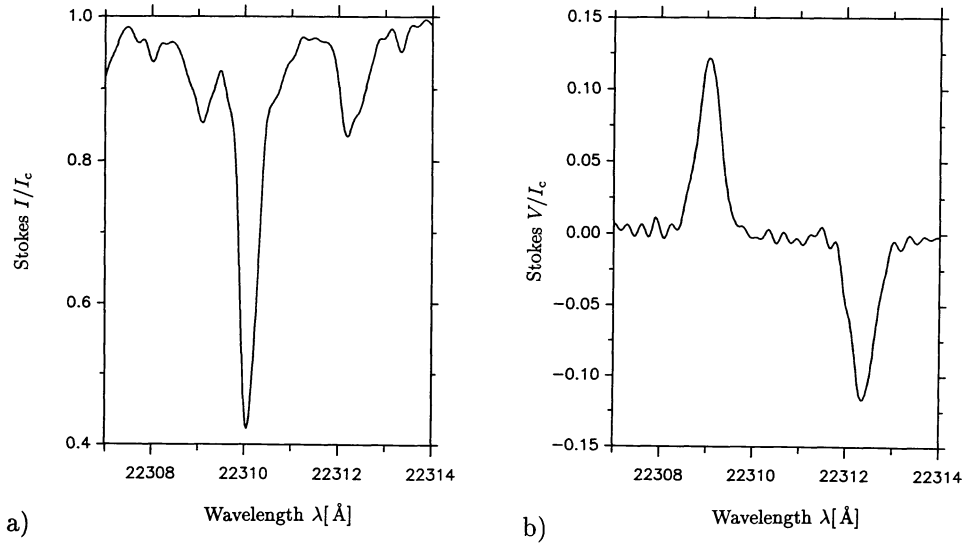

Fig. 2. a) Umbral Stokes I profile of Ti I 22310 Å. b) Corresponding Stokes V profile

unusable in its present state. Fortunately, there are ways of removing telluric blends, based on obtaining two different observations of the same wavelength range. The two observations must either be of the same solar spectrum but at different airmasses, i.e. different telluric line strengths, or of the same telluric spectrum but with the solar lines having vastly different strength. The former approach has been taken to produce spectral atlases free of telluric lines by Livingston & Wallace (1991), Wallace & Livingston (1992) and Wallace et al. (1993, 1994). The latter has been applied by Saar & Linsky (1985) to clean the Ti I multiplet of telluric blends in M star spectra. As a template they used Sirius or another hot star in which the Ti I lines are not present.

The procedure used by Saar & Linsky (1985), which has its roots in the spectral atlas of Hall (1974), consists of measuring as simultaneously as possible the spectra in the umbra and in a template where the Ti I lines completely disappear due to the increased temperature. If the telluric lines are equal in both spectra (i.e. if the airmass of water vapor is the same) then the telluric part is removed by simply dividing the two spectra, leaving the signal from the Ti I line alone. If the airmass is not equal, then the template spectrum must be transformed to the airmass of the umbral spectrum (see, e.g., Paper II). Since the lines of this Ti I multiplet are very weak in the quiet sun, we can apply the same technique as Saar & Linsky (1985) if we are willing to sacrifice some accuracy at line center. As a template we use the plage spectrum, which, due to the higher temperature in the line forming layers, is even cleaner than the quiet-sun spectrum. Figure 3 shows the same wavelength range as Fig. 2, but recorded in a plage. It is dominated by the blend at 22310 Å and also reveals a few other telluric lines that are present in the umbral profile as well. One of these is especially annoying due to its position in the red σ-component of the Zeeman split

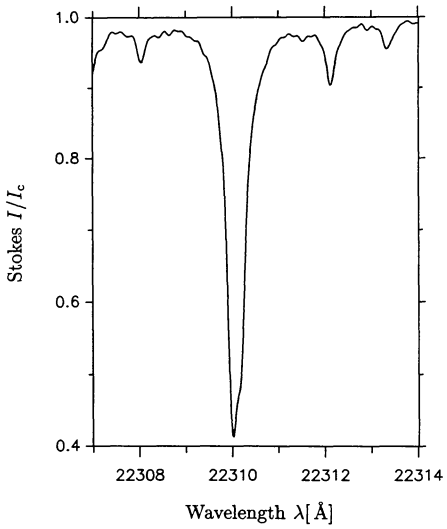

Fig. 3. Stokes I profile of Ti I 22310 Å observed in a plage

umbral profile. Fortuitously, the telluric lines have almost exactly the same strength in both spectra.

The result of the above procedure applied to the spectra in Figs. 2 and 3 is shown in Fig. 4, where the processed Stokes I umbral profile (upper curve) is plotted with the processed Stokes V umbral profile (lower curve). To correct for blends to both Stokes I and V simultaneously the above procedure was applied to $I+V$ and $I-V$ separately and I and V were formed after that. Stokes Q and U can also be freed from telluric blends in this manner. The effects of the unpolarized telluric blends on Stokes V are small, mainly because unpolarized lines affect Stokes V much less than Stokes I (Solanki et al. 1990, Paper I). Also, the blends are relatively weak at the wavelength of the σ-components. The maxima of the Stokes I and V σ-components now fall on exactly the same wavelengths.

The amplitude asymmetry between these two components also has the same trend in both spectra. This gives us confidence that the blends have been removed properly. The Stokes I π-component, which was before completely swamped by the telluric line, can now be seen. That this π-component is not an artifact can be confirmed simply by comparing the red flanks of the strongest telluric line in Figs. 2a and 3. That it is most probably not significantly affected by any minor Ti I signal remaining in the plage spectrum will be demonstrated below using another Ti I line. The main disadvantage of this procedure is that it increases the noise in the spectra, particularly at wavelengths at which the telluric absorption is large.

The inclination angle of the magnetic field can now be obtained from the σ-π amplitude ratio. The inclination angle with respect to the line-of-sight direction obtained from Fig. 4 is 33° compared to an inclination of 64° for the radial direction. It is important for the success of this diagnostic that the σ-π ratio is not affected by stray-light from the non-magnetic atmosphere, a condition that is easily fulfilled, since the line disappears outside sunspots.[2]

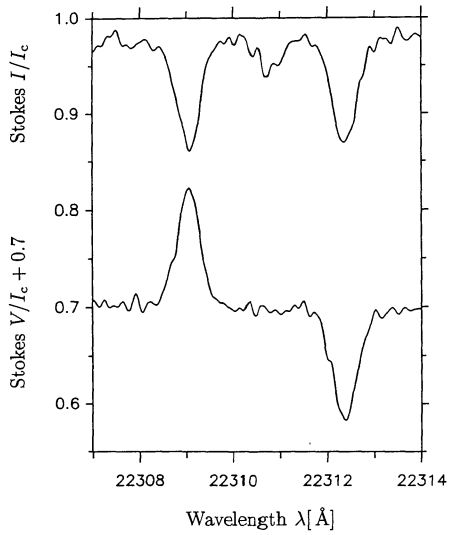

Fig. 4. Umbral Stokes I and V profiles of Ti I 22310 Å after removal of the telluric blends

The other lines in the Ti I multiplet are not normal Zeeman triplets and consequently possess broader σ-components than the $g = 2.5$ triplet (Ti I 22310 Å). Figure 5 illustrates the Stokes I and V profiles of the line with the smallest $g_{\rm eff}$ value. The half widths of the Stokes V σ-components of Ti I 22310 Å and Ti I 21897 Å are 0.43 Å and 0.86 Å respectively. The great advantage of having unsaturated lines belonging to the same multiplet with widely different Landé factors is that, as in the case of 15648 Å and 15652 Å, their combination allows the detection of any distribution (in the horizontal or vertical direction) of the magnetic field strength. The factor of 2.14 difference in $g_{\rm eff}$, the small non-magnetic line width and the absence of significant non-telluric blending (except in the blue wing of 21897 Å) should make the Ti I lines extremely sensitive in this respect. Actually, it may be possible, for sufficiently inclined fields, to constrain the magnetic distribution from the Ti I triplet alone, by comparing the width of its σ- with that of its π-component (Deming et al. 1988 and Hewagama et al. 1993 pioneered this approach for the 12 μm lines in sunspot penumbrae). If the σ-component is broader, then a magnetic field strength distribution is expected (although a field-aligned velocity might also cause such an effect, Zayer et al. 1989).

Another line of particular interest is Ti I 22211 Å, which exhibits two separate components in each lobe of the measured Stokes V profile (Fig. 6b). This line has the second largest Landé factor of the multiplet and is composed of the fewest different Zeeman components after the triplet. The corresponding measured Stokes I profile is the solid curve of Fig. 6a and is, like the triplet, strongly blended with telluric features. Here again the telluric-blend-removal works well, when applied separately to the observed Stokes $I+V$ and $I-V$ profiles, with Stokes I and V reconstructed therefrom after processing the blends. The resulting Stokes I and V profiles are represented in Figs. 6a and b by the dashed curves. These profiles are gratifyingly clean. In this case the Stokes V profile shows a substantial improvement after the blend removal. For example, the amplitude difference between the red and blue peaks is now no bigger than the noise in the data. Note the very clean continuum in the core of the line. The splitting pattern of this line is such that the π-component breaks up into sub-components that practically merge with the σ-components — the splitting pattern in the notation of Beckers (1969) is 100⟨1000⟩150(500)250(500). The presence of the π-component produces the slight bumps at the inner edge of the σ-components of the Stokes I profile, which (the bumps) are missing in the Stokes V profile. The clean continuum at line center is a good indicator that our basic assumption, namely that the line disappears outside the sunspot is fulfilled to a high degree (right down to the noise level). If it had not been fulfilled, then a spurious emission feature would have appeared in the core of the deblended profile.

5. The He I 10830 Å line

Figures 7a and 8a show the observed intensity of the He I 10830 Å line (solid curve) in an umbra and in a plage, respectively. The He I 10830 Å line is probably the best currently available diagnostic of upper chromospheric magnetic fields (cf. Harvey & Hall 1971 for the first magnetic

[2] There may possibly be some contamination from the penumbra, however. Nevertheless, this freedom from non-magnetic stray-light is a major advantage with respect to Fe I 15648 Å.

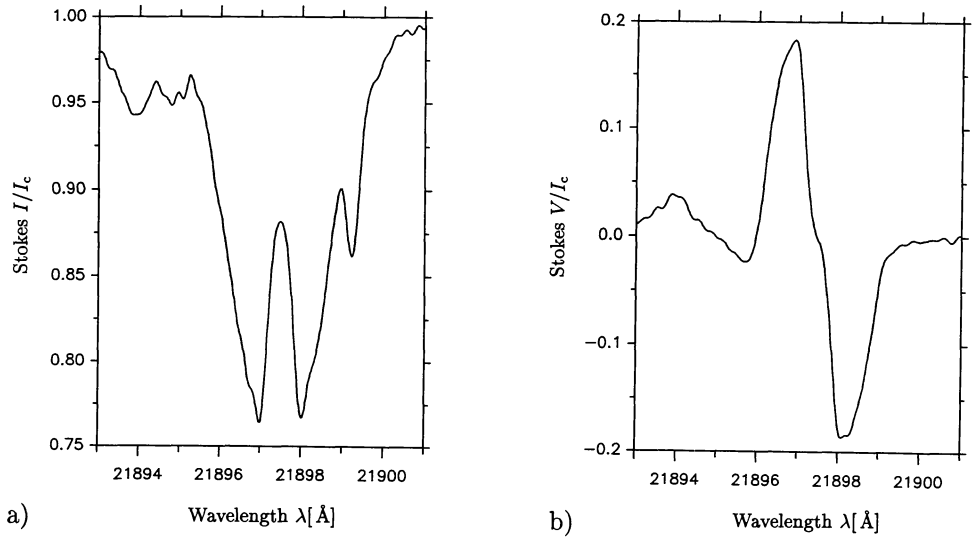

Fig. 5. Umbral Stokes I and V profiles of Ti I 21897 Å ($g_{\rm eff} = 1.167$)

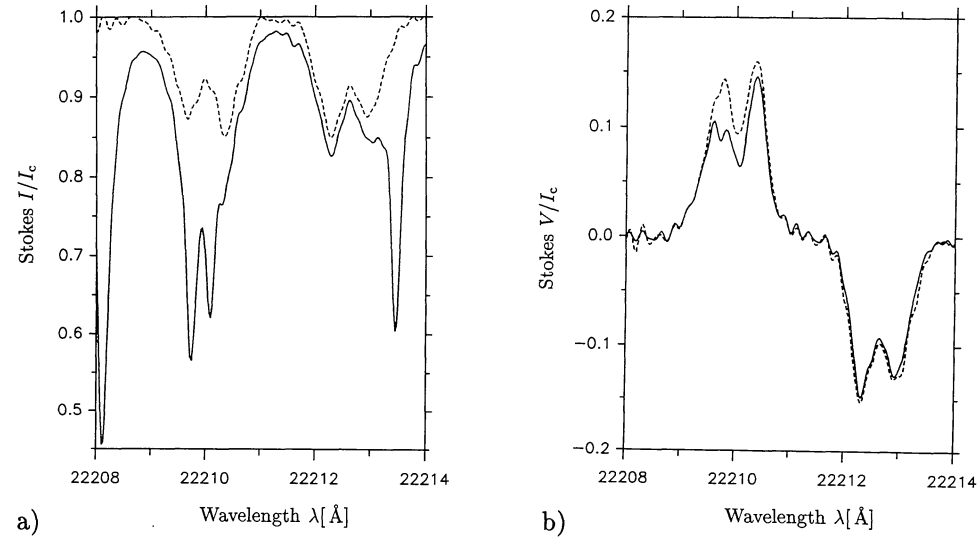

Fig. 6. a) Observed (solid) umbral Stokes I profile of Ti I 22211 Å ($g_{\rm eff} = 2.0$) and profile obtained therefrom after removal of the telluric blends (dashed). b) Corresponding Stokes V profiles

measurement using this line). It is formed over a narrow height range in the upper chromosphere without any contribution from the photosphere (e.g. Fontenla et al. 1993; Avrett et al. 1994). Its formation height has recently been estimated at 2400 km above $\tau_{5000} = 1$ from off-limb observations by Schmidt et al. (1994). It is relatively weak and optically thin in most solar features outside filaments (Giovanelli & Hall 1977). It is still in the weak field regime (i.e. $\Delta\lambda_{\rm H} < \Delta\lambda_{\rm D}$, where $\Delta\lambda_{\rm D}$ is the Doppler width of the line) even over umbrae (Rüedi et al. 1995). This line is actually composed of three individual components: located at 10830.34 Å, 10830.25 Å and 10829.08 Å. A water vapor blend is also located at the wavelength of the two strong components around 10830.30 Å (Giovanelli & Hall 1977).[3] Our data having been observed at a time of low water content of the earth's atmosphere are not significantly affected by this blend, but this might not always be the case and has to be taken into consideration when analyzing data recorded with larger amounts of water vapor. The solid curves in Fig. 7b and 8b are the corresponding observed Stokes V profiles.

In the weak field regime the Stokes V profile shape can be obtained from the Stokes I profile by differentiation. At first glance, it seems that the Stokes V profiles shown on Figs. 7b and 8b are more reminiscent of Stokes Q

[3] Note that in Rüedi et al. 1995 the wavelength position of the different components were slightly wrong, but the field strength value they derived are not affected by this imprecision.

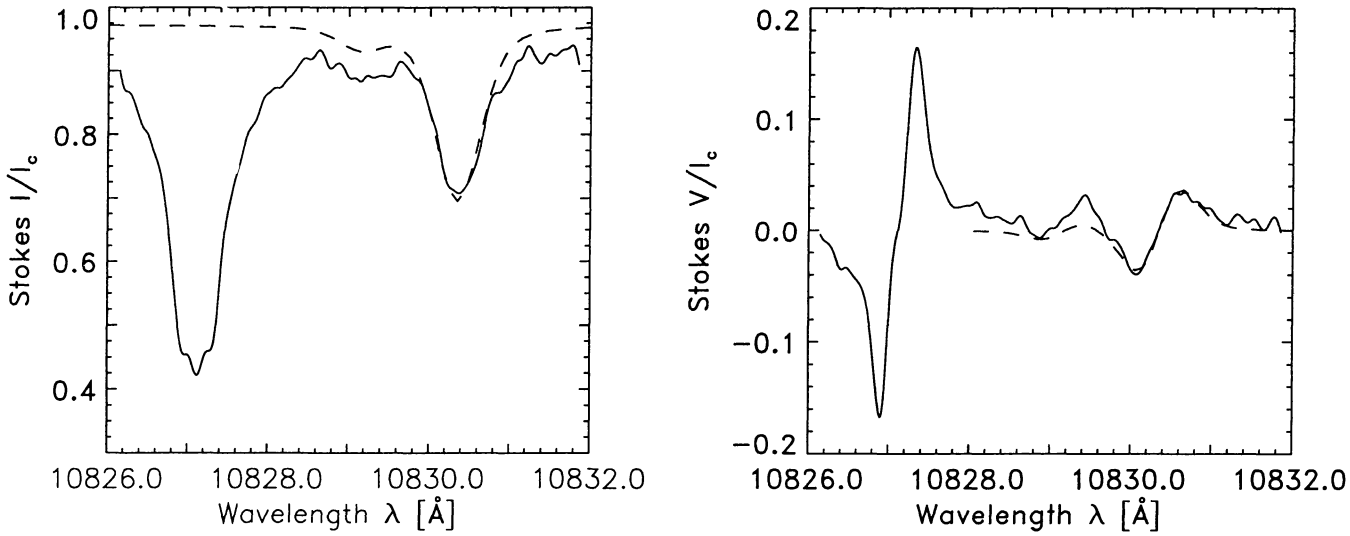

Fig. 7. a) Observed umbral Stokes I spectrum (solid) of He I 10830 Å and a fit to it (dashed). b) Corresponding Stokes V spectrum. See text for details

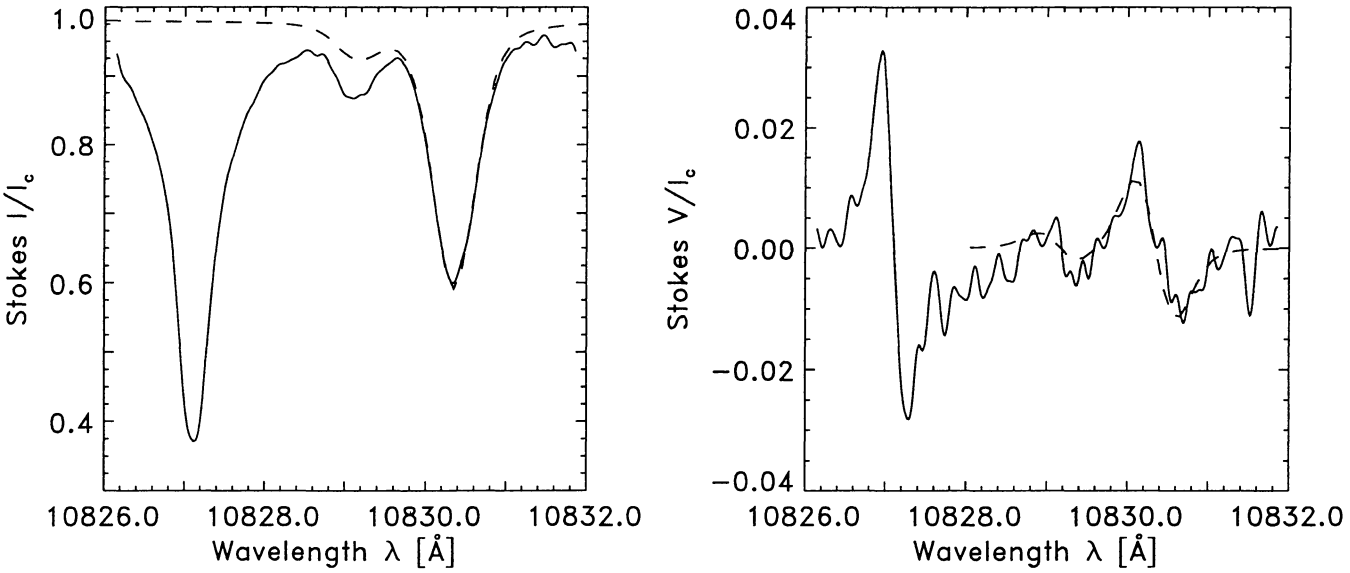

Fig. 8. Same as Fig. 7, but for a plage region

profiles, with their two σ-components and one π-component of opposite sign, than of a typical antisymmetric Stokes V profile. This is not an artifact of the measurement and does not imply the presence of two opposite polarity field components at the chromospheric level, but really has a correlation to the Stokes I derivative. Due to the different Landé factors of the different lines forming the He I triplet, each of these must be weighted by its Landé factor before differentiation. In order to simulate this fact we fitted the Stokes I profiles of these lines with a superposition of Voigt profiles whose areas are weighted by the oscillator strength of each of the transitions. These fits are represented by the dashed curves in Fig. 7a and 8a. We then multiplied each component by its Landé factor, added them together and finally differentiated this composite profile (see Rüedi et al. 1995 for details on the procedure). These synthetic Stokes V profiles are the dashed curves in Fig. 7b and 8b, which have been scaled to the amplitude of the red wing of the He I 10830.34 Å line in order to be as little affected as possible by a Ca-blend (10829.3 Å) which is responsible for the discrepancy between observed profile and fit of the weaker He I component. Assuming a filling factor of 1, representing a magnetic field spread evenly over the resolution element at upper chromospheric heights, it is straightforward to extract the magnetic field strength B from the scaling factor. A comparison of the field strength obtained with this line and with other photospheric lines gives a rough estimate

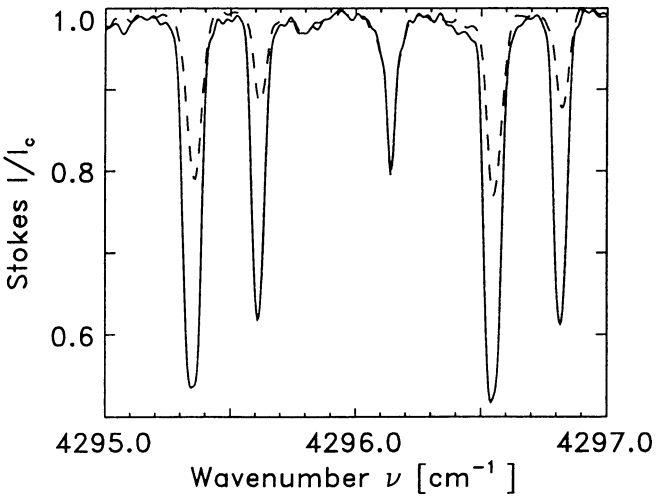

Fig. 9. CO first overtone vibration-rotation band lines observed in an umbra (solid) and in a plage (dashed). The wavenumber scale has been used to facilitate comparison with the data published by Ayres (1978)

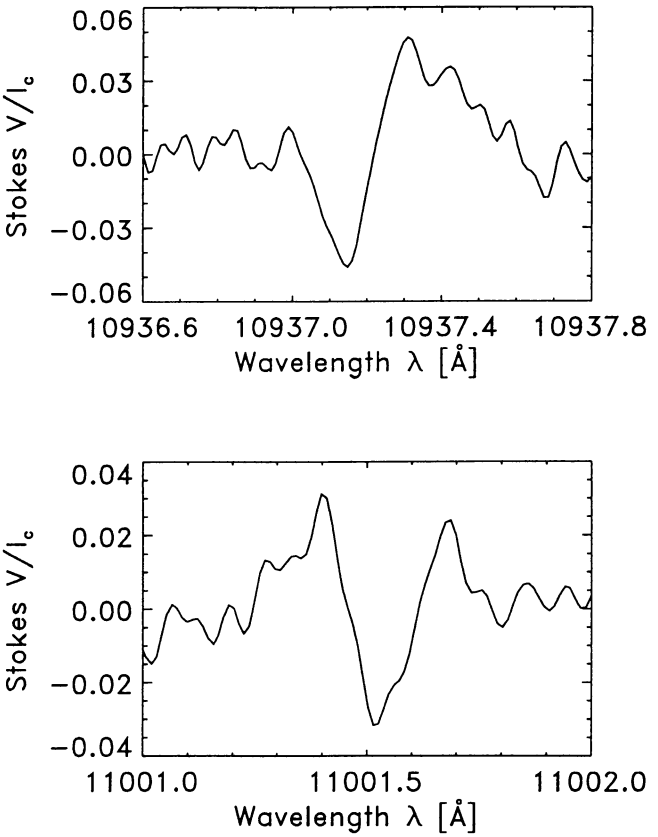

Fig. 10. Stokes V umbral profiles of two CN lines. a) CN 10937.23 Å, b) CN 11001.49 Å. Note the antisymmetric shape of the former and the symmetric shape of the latter profile

of the field strength gradient averaged over approximately 1500–2000 km (difference between heights of formation of the He I and photospheric lines, e.g. Fe I 15648 Å, Si I 12395.8 in plage, Fe I 12879.8 in the umbra). The upper chromospheric fields, measured with the He I line, are 190 G and 1400 G in the plage and in the umbral spectrum, respectively. For the photospheric field strength in the plage, we obtain $B = 1520$ G from Fe I 11422 Å ($g = 2$), and 1480 G from Si I 12395.8 Å ($g = 2$), which are typical for small-scale magnetic features. In the umbra Fe I 12879.8 Å ($g = 1.5$) was used and gave $B = 2610$ G. The corresponding gradient is approximately 0.6 Gkm^{-1} for both plage and umbra. For the umbra this result is in good agreement with previous measurements carried out over a similar height range (Abdussamatov 1971; Lee et al. 1993; Henze et al. 1982; Hagyard et al. 1983; Rüedi et al. 1995). For plages this is, to our knowledge, the first determination of the vertical field strength gradient over this height range. For more details on the diagnostic potential and analysis of this line we refer to Rüedi et al. (1995).

6. Other atomic lines of interest

High excitation C I lines prefer higher temperatures and are formed near $\tau_c = 1$, even deeper in the photosphere than the Fe I 15648 Å line (e.g. Van Ballegooijen 1984). The main use of these lines (besides providing estimates of the solar carbon abundance, Stürenburg & Holweger 1990; Grevesse et al. 1991) is expected to consist of providing information on the continuum contrast and thermal stratification in the lower photosphere of magnetic features (Van Ballegooijen 1984; Solanki & Brigljević 1992). Although a few high excitation C I lines are present in the optical solar spectrum, a larger number is present between 1.0 and 1.3 μm. Some of these lines (e.g. C I 10683.1 Å, $g_{\rm eff} = 1.0$, C I 10685.4 Å, $g_{\rm eff} = 0.5$, C I 10691.2 Å, $g_{\rm eff} = 1.167$, C I 10729.5 Å, $g_{\rm eff} = 1.333$) show Stokes V signals of amplitudes of 3–5% in both plages and umbra. Due to the low detector response at these wavelengths these profiles are relatively noisy in our data, but should be quite useful once data of better quality are available.

The Mg II lines at 10952 Å ($g_{\rm eff} = 0.839$) and 10914 Å ($g_{\rm eff} = 1.1$) exhibit considerable thermal sensitivity. They are much stronger in the plage and even disappear in the umbra. Unfortunately, they show no polarization signals above the noise.

7. Molecular lines

The numerous CN (in the J-band) and CO lines (in the K-band), as well as the OH lines (in the H-band) have the opposite temperature sensitivity to the Mg II lines – i.e. they are much stronger in the umbra. These lines can be used to derive thermal properties with considerable accuracy (photospheric stray-light should not be a major problem since these molecular lines are much stronger in

Table 3a. List of J-band lines (1.1 μm–1.3 μm)

1 $\lambda_\odot$ [Å]	2 $\sigma_\odot$ [cm^{-1}]	3 a_b(pla)	4 a_r(pla)	5 Blend Plage	6 a_b(umb)	7 a_r(umb)	8 Blend Umbra	9 Ion	10 λ_{lab} [Å]	11 Transition	12 χ_e [eV]	13 $g_{eff}^{calc.}$	14 $g_{eff}^{emp.}$	15 X_π	16 X_σ	17 Y_σ	18 λ_{calc} [Å]
13123.440	7617.870	6.2	4.7	0–1	7.8	7.8	1	Al I	13123.440	$4s\ ^2S_{1/2}$—$4p\ ^2P^o_{3/2}$	3.14	1.167		0.111	0.083	0.028	.411
12975.9	7704.5	*4.2	*4.4	0	7.8	7.5	0–1	Mn I	12975.89	$a\ ^4D_{7/2}$—$z\ ^4P^o_{5/2}$	2.89	1.214	1.211	0.066	0.050	0.010	
12899.7	7750.0	6.0	5.6	3	8.7	8.7	0–1	Mn I	12899.76	$a\ ^6D_{9/2}$—$z\ ^6P^o_{7/2}$	2.11	1.278	1.288	0.097	0.073	0.017	
12879.778	7761.986	6.4	5.3	3	8.6	8.2	0–1	Fe I	12879.769	$a\ ^3P_2$ —$z\ ^5D^o_3$	2.28	1.500	1.494	0.000	0.000	0.000	.761
12847.050	7781.759	*2.0	*1.8	0–1	8.9	8.7	0–1	Ti I	12847.029	$b\ ^3F_3$—$z\ ^3F^o_3$	1.44	1.083	1.075	0.000	0.000	0.000	.030
12831.414	7791.242	*1.0	*1.3	3	7.9	7.5	0	Ti I	12831.437	$b\ ^3F_2$—$z\ ^3F^o_2$	1.43	0.667	0.670	0.000	0.000	0.000	.437
12821.6	7797.2	*2.1	*2.2	1–2	9.0	9.0	1–2	Ti I	12821.67	$b\ ^3F^o_4$—$z\ ^3F_4$	1.46	1.250	1.260	0.000	0.000	0.000	.672
12638.717	7910.031	5.1	4.2	2–3	*6.0	*5.9	2	Fe I	12638.706	$y\ ^5P^o_3$ —$e\ ^5D_4$	4.56	1.250	1.264	0.083	0.063	0.014	.700
12522.16	7983.658	*2.7	*3.6	2–3	8.3	9.0	3	K I	12522.11	$4p\ ^2P^o_{3/2}$—$5s\ ^2S_{1/2}$	1.62	1.167		0.111	0.083	0.028	.111
12432.267	8041.385	*2.9	*2.2	1	8.2	7.7	1–2	K I	12432.244	$4p\ ^2P^o_{1/2}$—$5s\ ^2S_{1/2}$	1.61	1.333		0.444	0.000	0.000	.274
12395.838	8065.017	5.3	4.2	0–1	*2.5	*2.4	2	Si I	12395.834	$4s\ ^3P^o_2$—$4p\ ^3D_1$	4.95	2.000		0.600	0.450	−0.300	.832
12270.712	8147.257	5.8	4.0	3	*5.8	*5.7	1	Si I	12270.693	$4s\ ^3P^o_2$—$4p\ ^3D_2$	4.95	1.333		0.378	0.117	0.000	.693
12031.527	8309.223	5.6	4.2	2	*6.3	*6.3	2–3	Si I	12031.517	$4s\ ^3P^o_2$—$4p\ ^3D_3$	4.95	1.167		0.044	0.033	0.006	.504
11949.742	8366.092	—	—	3	7.3	7.5	0	Ti I	11949.54	$b\ ^3F_3$—$z\ ^3D^o_2$	1.43	0.917	0.915	0.011	0.008	0.001	.542
11884.102	8412.300	7.3	5.6	0	*6.7	*7.4	1–2	Fe I	11884.085	$a\ ^5P_1$—$z\ ^5D^o_2$	2.22	1.000	1.005	0.600	0.450	0.300	.082
11882.859	8413.181	6.9	5.1	0–1	7.6	7.4	2–3	Fe I	11882.847	$a\ ^5P_2$—$z\ ^5D^o_3$	2.20	1.167	1.180	0.178	0.133	0.044	.837
11838.944	8444.352	5.1	3.6	0–1	*2.7	*2.6	1–2	Ca II	11838.997	$5s\ ^2S_{1/2}$—$5p\ ^2P^o_{3/2}$	6.47	1.167		0.111	0.083	0.028	.997
11783.289	8484.272	6.4	5.1	0	8.6	8.3	0	Fe I	11783.267	$b\ ^3P_2$—$z\ ^3D^o_3$	2.83	1.167	1.144	0.044	0.033	0.006	.261
11772.77	8491.853	2.4	5.1	2–3	6.1	9.9	1–2	K I	11772.83	$4p\ ^2P^o_{3/2}$—$3d\ ^2D_{5/2}$	1.62	1.100		0.019	0.014	0.002	.830
11689.981	8551.993	—	—	3	8.2	7.3	3	Fe I	11689.976	$a\ ^5P_1$—$z\ ^5D^o_1$	2.22	2.000	1.997	1.000	0.250	0.000	.971
11638.232	8590.019	7.6	6.2	3	9.4	9.2	2	Fe I	11638.264	$a\ ^5P_3$—$z\ ^5D^o_3$	2.18	1.583	1.583	0.194	0.063	0.000	.258
11610.59	8610.47	5.1	3.6	2	8.6	7.1	2–3	Cr I	11610.52	$z\ ^5P^o_3$ —$c\ ^5D_4$	3.32	1.250	1.245?	0.083	0.063	0.014	
11607.585	8612.699	7.1	6.9	0	9.4	9.4	0	Fe I	11607.575	$a\ ^5P_2$—$z\ ^5D^o_2$	2.20	1.667	1.662	0.378	0.117	0.000	.570
11593.618	8623.074	10.0	7.1	2–3	9.0	4.2	3	Fe I	11593.591	$a\ ^5P_1$—$z\ ^5D^o_0$	2.22	2.500	2.499?	0.000	0.000	0.000	.584
11422.333	8752.383	9.3	7.8	0-1	10.0	9.8	1–2	Fe I	11422.323	$a\ ^5P_2$—$z\ ^5D^o_1$	2.20	2.000	1.983	0.067	0.050	−0.011	.317
11403.80	8766.606	6.0	5.1	2	7.0	8.5	3	Na I	11403.78	$3p\ ^2P_{3/2}$—$4s\ ^2S_{1/2}$	2.10	1.167		0.111	0.083	0.028	.783
11119.803	8990.502	5.3	5.3	0	*7.3	*6.9	1	Fe I	11119.798	$b\ ^3P_1$—$z\ ^3D^o_1$	2.85	1.000	1.001	1.000	0.250	0.000	.797
11015.531	9075.606	5.3	4.9	2–3	*7.8	*6.0	3	Cr I	11015.62	$y\ ^7P^o_3$ —$e\ ^7S_3$	3.45	1.958	1.965?	0.049	0.016	0.000	.66

Table 3b. List of H-band lines (1.4 μm – 1.7 μm)

1 $\lambda_\odot$ [Å]	2 $\sigma_\odot$ [cm^{-1}]	3 a_b(pla)	4 a_r(pla)	5 Blend Plage	6 a_b(umb)	7 a_r(umb)	8 Blend Umbra	9 Ion	10 λ_{lab} [Å]	11 Transition	12 χ_e [eV]	13 $g_{eff}^{calc.}$	14 $g_{eff}^{emp.}$	15 X_π	16 X_σ	17 Y_σ	18 λ_{calc} [Å]
16763.361	5963.762	*5.6	*5.2	0–1	7.1	7.2	1	Al I	16763.366	$4p\ ^2P^o_{3/2}$—$4d\ ^2D_{3/2}$	4.09	1.067		0.583	0.171	0.000	.360
16750.614	5968.300	6.8	7.1	3	6.3	6.6	1–2	Al I	16750.587	$4p\ ^2P^o_{3/2}$—$4d\ ^2D_{5/2}$	4.09	1.100		0.019	0.014	0.002	.564
16680.809	5993.276	8.1	7.7	0–1	*5.8	*6.3	1–2	Si I	16680.77	$4p\ ^3D_3$—$3d\ ^3D^o_3$	5.98	1.333		0.000	0.000	0.000	.770
16486.686	6063.844	7.1	6.8	0–1	6.5	6.2	0–1	Fe I	16486.669	$e\ ^5F_5$—$3d^74p\ ^5G^o_6$	5.83	1.167	1.114?	0.031	0.023	0.003	.691
16444.840	6079.274	8.1	7.7	0	6.9	7.	2	Fe I	16444.818	$e\ ^5F_5$—$3d^74p\ ^5F^o_5$	5.83	1.400	1.410?	0.000	0.000	0.000	.816
16241.866	6155.246	7.4	6.8	1–2	*3.8	*4.6	2–3	Si I	16241.84	$4p\ ^3D_2$—$3d\ ^3D^o_3$	5.96	1.500		0.044	0.033	−0.006	.83
16197.040	6172.281	—	—	1	7.3	6.7	3	Ca I	16197.075	$4s5p\ ^3P^o_2$—$4s5d\ ^3D_3$	4.53	1.167		0.044	0.033	0.006	.075
16157.3	6187.46	*3.5	*3.7	1–2	5.5	7.7	2	Ca I	16157.36	$4s5p\ ^1P^o_1$—$4s5d\ ^1D_2$	4.55	1.000		0.000	0.000	0.000	.364
16150.763	6189.967	*3.4	*3.5	0–1	6.3	6.7	1–2	Ca I	16150.763	$5p\ ^3P^o_1$—$5d\ ^3D_2$	4.53	1.000		0.067	0.050	0.011	.763
16102.413	6208.553	7.1	6.4	0	*6.1	*6.2	1–2	Fe I	16102.408	$e\ ^5F_4$—$5p\ ^5G^o_5$	5.87	1.100	1.138?	0.033	0.025	0.003	.450
15868.544	6300.054	7.4	6.8	0	6.6	6.3	1–2	Fe I	15868.526	$e\ ^5D_3$—$t\ ^5D^o_3$	5.59	1.500	1.504?	0.000	0.000	0.000	.522
15723.609	6358.126	8.1	7.1	0–1	6.8	7.1	1–2	Fe I	15723.593	$e\ ^5D_2$—$u\ ^5P^o_3$	5.62	1.833	1.830?	0.044	0.033	−0.006	.591
15715.	6362.	*2.1	*1.4	3	9.3	4.3	3	Ti I	15715.57	$a\ ^3G_3$—$z\ ^3G^o_3$	1.87	0.750	0.745	0.000	0.000	0.000	.573
15662.018	6383.124	7.4	6.4	1–2	4.9	6.6	0–1	Fe I	15662.018	$e\ ^5F_5$—$3d^74p\ ^5F^o_4$	5.83	1.500	1.563?	0.012	0.009	−0.001	
15631.960	6395.403	9.0	7.7	2–3	7.2	6.3	1–2	Fe I	15631.950	$e\ ^7D_4$—$n\ ^7D^o_4$	5.35	1.650	1.653?	0.000	0.000	0.000	.975
15621.679	6399.612	8.1	2.4	1	6.9	7.3	0	Fe I	15621.659	$e\ ^5D_4$—$t\ ^5D^o_4$	5.54	1.500	1.494	0.000	0.000	0.000	.664
15543.779	6431.685	*2.4	*1.9	0	9.9	10.0	1–2	Ti I	15543.68	$a\ ^3G_4$—$z\ ^3G^o_4$	1.88	1.050	1.060	0.000	0.000	0.000	.720
15334.8	6519.3	—	—	3	9.8	5.8	3	Ti I	15334.84	$a\ ^3G_5$—$z\ ^3G^o_5$	1.89	1.200	1.210	0.000	0.000	0.000	.847
15294.584	6536.476	8.1	7.1	3	6.9	7.2	1	Fe I	15294.562	$e\ ^7D_5$—$n\ ^7D^o_5$	5.31	1.600	1.593?	0.000	0.000	0.000	.582
15244.988	6557.741	7.4	7.1	0–1	*4.6	*6.0	1–2	Fe I	15244.973	$e\ ^5D_3$—$u\ ^5F^o_3$	5.59	1.375	1.379?	0.438	0.141	0.000	.965
15219.637	6568.664	8.1	7.1	1	*5.8	*6.4	0–1	Fe I	15219.622	$e\ ^5D_3$—$t\ ^5D^o_2$	5.59	1.500	1.516?	0.000	0.000	0.000	.621
15207.545	6573.887	8.7	8.4	0	6.6	7.1	0–1	Fe I	15207.530	$e\ ^7D_3$—$n\ ^7D^o_2$	5.39	1.500	1.510?	0.100	0.075	0.019	.547
15051.765	6641.924	9.0	9.0	1–2	6.5	7.1	1	Fe I	15051.749	$e\ ^7D_4$—$n\ ^7D^o_3$	5.35	1.500	1.513	0.030	0.023	0.003	.770
15047.644	6643.743	9.0	7.4	3	6.9	6.7	0–1	Mg I	15047.715	$4s\ ^3S_1$—$4p\ ^3P^o_0$	5.11	2.000		0.000	0.000	0.000	.705
14956.166	6684.379	9.0	5.5	2	*6.1	*6.0	2	Fe I	14956.151	$e\ ^5D_4$—$t\ ^5D^o_3$	5.54	1.500	1.505?	0.000	0.000	0.000	.150
14826.468	6742.852	10.0	7.1	3	6.7	2.3	1–2	Fe I	14826.412	$e\ ^7D_5$—$5p\ ^7D^o_4$	5.31	1.500	1.445	0.012	0.009	0.001	.437
14652.917	6822.715	8.4	8.1	1	*3.9	*3.9	1–2	Fe I	14652.901	$n\ ^7F^o_5$—$5d\ ^7G_6$	6.20	1.167		0.063	0.048	0.009	

Table 3c. List of K-band lines (1.9 μm–2.5 μm)

1	2	3	4	5	6	7	8	9	10	11	12	13	14	15	16	17	18
$\lambda_\odot$ [Å]	$\sigma_\odot$ [cm^{-1}]	a_b(pla)	a_r(pla)	Blend Plage	a_b(umb)	a_r(umb)	Blend Umbra	Ion	λ_{lab} [Å]	Transition	χ_e [eV]	$g_{eff}^{calc.}$	$g_{eff}^{emp.}$	X_π	X_σ	Y_σ	λ_{calc} [Å]
24281.8	4117.2	—	—	—	7.5	6.9	1–2	Ti I	24281.84	$b\ ^1G_4 - z\ ^1F_3^\circ$	2.27	1.000	1.050	0.000	0.000	0.000	.808
23441.3	4264.8	—	—	0–1	7.5	7.2	1–2	Ti I	23441.46	$a\ ^3G_4 - z\ ^3F_3^\circ$	1.88	1.000	1.045	0.003	0.003	0.000	.472
23379.28	4276.125	3.8	2.5	3	*6.6	*6.2	3	Na I	23379.14	$4p\ ^2P_{3/2} - 4d\ ^2D_{5/2}$	1.89	1.167		0.021	0.016	0.002	.142
22963.2	4353.6	—	—	2–3	8.6	9.1	2–3	Ti I	22963.33	$a\ ^3G_5 - z\ ^3F_4^\circ$	1.89	1.100	1.100	0.012	0.009	0.001	.336
22651.27	4413.56	4.7	4.3	0–1	8.5	8.0	2–3	Ca I	22651.23	$4s4d\ ^3D_3 - 4s4f\ ^3F_4^\circ$	4.68	1.125		0.021	0.016	0.002	.178
22624.96	4418.69	4.3	4.9	1–2	8.1	6.4	2–3	Ca I	22624.93	$4s4d\ ^3D_2 - 4s4f\ ^3F_3^\circ$	4.68	1.000		0.011	0.008	0.001	.962
22619.853	4419.689	5.0	5.0	1–2	*6.6	*6.9	1–2	Fe I	22619.837	$x\ ^5F_5^\circ - e\ ^5D_4$	4.99	1.200	1.166	0.048	0.036	0.006	.813
22607.9	4422.0	4.3	3.4	3	6.7	7.3	2–3	Ca I	22607.93	$4s4d\ ^3D_1 - 4s4f\ ^3F_2^\circ$	4.68	0.750		0.017	0.013	−0.001	.945
22473.274	4448.516	4.6	3.9	3	*4.7	*4.8	3	Fe I	22473.278	$n\ ^7D_5^\circ - g\ ^7D_5$	6.12	1.600	1.593?	0.000	0.000	0.000	.324
22380.817	4466.893	4.6	4.6	1–2	*6.3	*6.2	0	Fe I	22380.797	$x\ ^5F_4^\circ - e\ ^5D_3$	5.03	1.125	1.058	0.067	0.051	0.010	.792
22274.0	4488.3	—	—	—	8.1	7.9	3	Ti I	22274.02	$a\ ^5P_3 - z\ ^5D_3^\circ$	1.75	1.583	1.575	0.194	0.063	0.000	.012
22257.122	4491.718	3.9	3.8	1	*5.3	*4.8	1	Fe I	22257.107	$x\ ^5F_3^\circ - e\ ^5D_2$	5.06	1.000	1.005	0.100	0.075	0.019	.097
22232.8	4496.6	—	—	—	8.0	8.3	1	Ti I	22232.83	$a\ ^5P_2 - z\ ^5D_2^\circ$	1.74	1.667	1.660	0.378	0.117	0.000	.839
22211.25	4500.99	—	—	—	6.9	6.9	3	Ti I	22211.23	$a\ ^5P_1 - z\ ^5D_1^\circ$	1.73	2.000	2.075	1.000	0.250	0.000	.228
22083.93	4526.944	4.4	4.8	0	9.0	9.1	0	Na I	22083.66	$4s\ ^2S_{1/2} - 4p\ ^2P_{1/2}$	3.19	1.333		0.444	0.000	0.000	.657
22062.84	4531.71	3.4	3.6	1–2	—	—	1–2	Si I	22062.71	$3d\ ^3D_3 - 4fF(7/2)_4$	5.62						.749
22056.62	4532.549	4.7	5.1	0–1	7.8	7.6	0–1	Na I	22056.40	$4s\ ^2S_{1/2} - 4p\ ^2P_{3/2}$	3.19	1.167		0.111	0.083	0.028	.304
22052.	4533.	—	—	—	7.0	5.5	2	Sc I	22052.1	$a\ ^4F_{9/2} - z\ ^4D_{7/2}^\circ$	1.45	1.167	1.141	0.035	0.026	0.004	.1
22004.5	4543.3	—	—	—	8.0	7.5	2–3	Ti I	22004.50	$a\ ^5P_1 - z\ ^5D_2^\circ$	1.73	1.000	1.000	0.600	0.450	0.300	.495
21897.4	4565.5	*1.1	*1.0	0–1	8.6	8.8	1–2	Ti I	21897.3	$a\ ^5P_2 - z\ ^5D_3^\circ$	1.74	1.167	1.160	0.178	0.133	0.044	.377
21879.45	4569.252	4.2	4.1	0–1	*3.7	*3.4	1–2	Si I	21879.35	$3d\ ^3D_2 - 4fF(5/2)_3$	5.62						.363
21782.94	4589.50	*2.0	*2.0	0–1	9.7	10.0	0–1	Ti I	21782.94	$a\ ^5P_3 - z\ ^5D_4^\circ$	1.75	1.250	1.285	0.083	0.063	0.014	.926
21354.32	4681.252	4.2	4.5	1	*3.4	*4.1	1–2	Si I	21354.20	$4p\ ^1D_2 - 5s\ ^1P_1^\circ$	6.22	1.000		0.000	0.000	0.000	.254
21163.827	4723.754	4.1	5.3	3	6.8	7.8	1	Al I	21163.799	$4p\ ^2P_{3/2}^\circ - 5s\ ^2S_{1/2}$	4.09	1.167		0.111	0.083	0.028	.323
21093.056	4739.603	4.3	4.7	2	7.9	8.7	1–2	Al I	21093.077	$4p\ ^2P_{1/2}^\circ - 5s\ ^2S_{1/2}$	4.09	1.333		0.444	0.000	0.000	.030
19862.2	5033.3	6.9	8.2	2	*6.9	*6.9	2–3	Ca I	19862.22	$4s4p\ ^3P_2^\circ - 4s3d\ ^3D_2$	1.90	1.333		0.378	0.117	0.000	.192
19853.02	5035.64	5.5	6.0	1–2	*6.5	*6.8	0–1	Ca I	19853.10	$4s5s\ ^3S_1 - 4s5p\ ^3P_2^\circ$	3.91	1.250		0.150	0.112	0.038	.092
19815.0	5045.3	5.0	5.3	0–1	7.5	7.5	0	Ca I	19815.02	$4s4d\ ^1D_2 - 4s4f\ ^1F_3^\circ$	4.62	1.000		0.000	0.000	0.000	.018
19791.	5051.	5.9	4.1	3	6.9	5.3	2	Fe I	19791.864	$x\ ^5D_4^\circ - e\ ^5D_4$	4.91	1.500	1.495	0.000	0.000	0.000	.877
19776.67	5055.08	7.3	10.0	1	7.2	7.4	2–3	Ca I	19776.79	$4s4p\ ^3P_2^\circ - 4s3d\ ^3D_3$	1.90	1.167		0.044	0.033	0.006	.772

the umbra than in the quiet sun or in the plage surrounding the sunspot). In regions with small-scale magnetic features, however, these lines can only provide spatially averaged information on the temperature, which must then be interpreted in terms of, e.g., a two component model (Ayres et al. 1986) that cannot give unique results for each component (Solanki et al. 1994a). Figure 9 shows, besides a telluric line in the middle of the plot, 4 CO-lines recorded in a plage (dashed) and in an umbra (solid). The umbral lines are 2–3 times stronger due to the cooler atmosphere and the thereby enhanced CO formation. We do find one odd effect, however. Solar plages are generally hotter than the quiet sun in the upper photospheric layers in which the CO lines are formed. Consequently molecular lines should be stronger in the quiet sun than in the plage, as confirmed by the observations of, e.g., Ayres et al. (1986). Our observed plage profiles of CO, however, are deeper than the quiet sun profiles observed by Ayres (1978) at the same μ. The most reasonable explanation to this enigma is that a (small) pore may have been present in the resolution element of our 'plage' observation which was located close to the analyzed sunspot (NOAA 6469) and may have escaped detection due to the poor seeing.

The polarization properties of the CN lines were first observed by Harvey (1973). He noted that some of these lines exhibit very asymmetrical Stokes V profiles. We also see polarized signals which reach up to 5% of the continuum intensity from the lines of his list in our umbral spectrum. A typical Stokes V signal of the R_2 branch is plotted in Fig. 10a. In spite of its asymmetry, this line still shows a Stokes V profile of the usual antisymmetric shape. In the R_1 and Q_1 branches, however, some lines behave as if they had a negative Landé factor and others, like CN 10985.48 Å, CN 11001.49 Å and CN 11028.79 Å, have Stokes V profiles that are symmetric and reminiscent of Stokes Q profiles rather than of Stokes V profiles. An example is shown in Fig. 10b. Note that according to Paper II all three CN lines mentioned above are unblended.

We confirm the observation made by Harvey (1985) that the two OH line pairs, one at 15422.4 Å and 15419.6 Å and the other at 15409.3 Å and 15407.43 Å show opposite Stokes V polarities, i.e. have Landé factors of opposite signs. In the absence of instrumental cross-talk (which is the case for our observations) these four Stokes V profiles are relatively antisymmetric. Any instrumental cross-talk from Stokes Q or U into Stokes V would make the Stokes V profiles of the two line pairs asymmetric in opposite directions. Conversely Stokes V into Stokes Q or U cross-talk should introduce opposite asymmetries into Stokes Q or U. Thus these lines provide many particularly sensitive probes of at least part of the Muller matrix of the observing setup, if the observed magnetic fields are sufficiently transverse.

8. Lines with strong Stokes V profiles

Considerable information on solar magnetic features is encoded in the profile shapes of Stokes parameters and in the ratios between two Stokes parameters or between different spectral lines. Therefore, of particular interest are lines exhibiting large Stokes V or Q signals, since for many observations only these lines possess a sufficient S/N ratio to allow a detailed analysis. Tables 3a to 3c list the lines showing the strongest Stokes V amplitudes in each FTS spectrum. The 20 lines with strongest Stokes V in the plage and the 20 strongest umbral Stokes V profiles within each spectral range have been included. Columns 1 and 2 give the solar wavelength in air and the corresponding wavenumber in vacuum. For almost all the lines these values were derived from the spectral atlas of Delbouille et al. (1981) whose wavenumber scale is corrected for the sun-observer relative motion and solar rotation (but not for gravitational redshift). The relative accuracy is lower for strongly blended lines. The conversion from wavenumber to wavelength is made using Edlén's (1953) formula. Columns 3 and 4 list the peak amplitude of the blue a_b and red a_r Stokes V wing, respectively, in the plage measurements. These values have been normalized such that the strongest amplitude in this spectrum has the value 10. This normalization was introduced in order to avoid confusion, since the J, H and K band spectra were not recorded simultaneously and thus do not correspond to exactly the same magnetic inclination angle and filling factor. Columns 6 and 7 list the similarly normalized a_b and a_r for the umbral data. In the umbral lists we have included the amplitude values of the strongest plage Stokes V profiles when they showed a detectable umbral signal and vice versa. These values are indicated by a star. In Cols. 5 and 8 an estimate of the blending index derived from the Stokes I profile is given. It varies from 0 for unblended to 3 for completely blended lines (see Papers I and II for details). This blending index refers primarily to Stokes I. If the blend is caused by an unpolarized line then the appropriate blending index for Stokes V may be reduced by an appropriate treatment.[4] Columns 9 and 10 list the ion and the wavelength as observed in the laboratory, while Col. 11 gives the transitions. The excitation potential of the lower level, in eV, is tabulated in Col. 12. The effective Landé factors, $g_{\rm eff}$, as computed employing LS-coupling values of g_u and g_l are to be found in Col. 13. Here g_u and g_l are the Landé factors of the upper and lower level, respectively. The $g_{\rm eff}$ listed in Col. 14 have been calculated using g_u and g_l values measured in the laboratory. The values followed by a question mark indicate transitions for which the Landé factor of only one level is known from laboratory measurements. The missing Landé factor is replaced by its LS-coupling value. Columns 15-17 give the second and third order coefficients X_π, X_σ and Y_σ of the expansion of a spectral line according to its Zeeman moments (cf. Landi Degl'Innocenti 1985; Mathys & Stenflo 1987). Finally, in the last column the final digits of the wavelength, as calculated from the energy difference between the transition levels, are given.

Surprisingly, only 12 out of 20 of the lines found to be strong in the plage region between 1.4 and 1.7 μm are also present in the network list of Solanki et al. (1990). This may have to do with the possibly present pore in the current plage spectrum.

9. Lines with strong Stokes Q profiles

Lines with strong Stokes Q were selected in the same manner as the Stokes V lines. Tables 4a and 4b list the lines showing the strongest Stokes Q amplitudes in the plage irrespective of whether it is the σ- or the π-component that has the larger amplitude. In these Tables the ions are listed in Col. 1, the solar wavelength in Col. 2 and the transition in Col. 3. Column 4 contains the effective Landé factors as calculated from LS-coupling. The amplitudes of the blue σ-component $a_b(\sigma)$, π-component $a(\pi)$ and red σ-component $a_r(\sigma)$ are tabulated in Cols. 5-7, respectively, normalized in the same manner as the Stokes V amplitudes in Table 3. Finally, the blending index is given in the last column.

The lines with large Stokes Q in the J-band are generally strong lines, but not necessarily so in the H-band. On the other hand, the lines in Table 4b (Stokes Q; average $g_{\rm eff}$ value 1.7) tend to have a larger $g_{\rm eff}$ than the lines in Table 3b (Stokes V; average 1.4). This reflects the different dependences of Stokes V and Q on B. In the weak-field limit, in or close to which most lines with $g_{\rm eff} < 1$ are, Stokes $Q \sim g^2B^2$ while Stokes $V \sim gB$. The Stokes Q and V amplitudes of completely split lines, on the other hand, are independent of B. The $g = 3$ line at 15648.5 Å does not have a sufficiently strong Stokes V to be listed in Table 3, but exhibits the second strongest Stokes Q profile in its wavelength range. This is empirical support for the prediction by Solanki et al. (1992a) that this line should be of particular value for measuring vector magnetic fields. This observation also implies that whereas most H-band Stokes V profiles with $g_{\rm eff} \gtrsim 1.5$ are completely split, this is not the case for the Stokes Q profiles, due to the π-component.

The data also provide us with other lines that should be particularly useful for measuring vector magnetic fields. We have selected the following 4 lines as being nearly ideal in the sense that they show large Stokes V and Q amplitudes and are practically unblended in both plage and

[4] It may appear strange that many lines have a larger blending index for the plage spectrum than for the umbral spectrum. This has to do with the fact that most lines are considerably stronger in the umbra and a small blend in the line profile is less visible. In addition, the umbral spectrum has more noise, which also reduces the visibility of small blends.

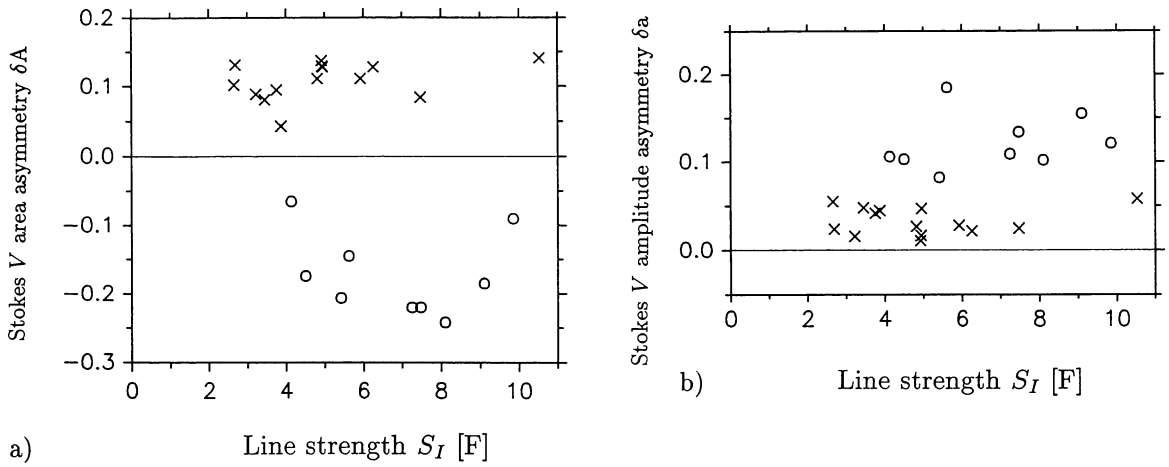

Fig. 11. a) Plage Stokes V relative area-asymmetry δA vs line strength S_I (F). See text for definitions. b) amplitude-asymmetry δa vs S_I. The crosses stand for the H-band data, the circle for the J-band data

umbra: Fe I 11607.6 Å, Fe I 11783.3 Å, Fe I 15207.5 Å and Fe I 15219.6 Å. Among these, 11783.3 Å exhibits the smallest splitting, making it a lesser choice in that respect. Other lines, which are less pure in either plage or umbra, but may still be of great use in the other type of magnetic features are: Fe I 11882.8 Å, Fe I 11884.1 Å, Fe I 12879.8 Å, Fe I 15245.0 Å, Fe I 15662.0 Å and 15723.6 Å. The Al I 13123.4 Å line in principle also belongs to this class, but according to Biémont & Brault (1987) is a blend of different hyperfine components and is perhaps better avoided.

The newest identification of Fe I 15692.77 Å by Litzén (1976) has a Landé factor of 0, which is incompatible with the observation of a Stokes Q signal. For that reason, the identification by Litzén & Vergès (1976) has been preferred and is listed in this table.

It is possible that lines with strong Stokes V or Q lying at the very edge of an observed spectral range are missing from the tables due to the reduced sensitivity of the detector or the reduced throughput of the predispersor (which greatly increases the noise).

10. Stokes V asymmetry

An examination of Tables 3a-c shows that the blue and red amplitudes of most lines, including the unblended lines, are similar for the sunspot data, but are not the same in the plage spectra. To illustrate this, we plot in Fig. 11a and 11b the plage Stokes V relative area- and amplitude-asymmetries (for lines in Table 3 with blending index less than two), against the line strength S_I (represented by the area of the lower half of the line, expressed in Fraunhofer, F). The relative amplitude asymmetry is defined as $\delta a = \frac{a_b - a_r}{a_b + a_r}$, where $a_{b,r}$ are, respectively, the peak amplitudes of the blue and red wings of Stokes V. The area asymmetry is defined similarly: $\delta A = \frac{A_b - A_r}{A_b + A_r}$, where $A_{b,r}$ are the areas of the blue and red wings of Stokes V. We have used the same definition as in previous work in order to be able to compare with it. The circles represent the J-band data, the crosses stand for H-band data.

Examples of Stokes V plage profiles typical for their spectral ranges $1.1 - 1.3$ μm and $1.4 - 1.7$ μm are plotted in Figs. 12a and 13a, respectively, while Figs. 12b and 13b show their Stokes Q counterparts. Note the difference in Stokes V and Q profile shapes. Particularly noteworthy is the shape of the Fe I 11783.3 Å line. The combination of significant positive δa and large negative δA, quite common to this spectral range, has not been observed before and gives the lines with large Stokes V in this spectrum quite a distinctive appearance. The most notable feature is the difference in width of the blue and red Stokes V lobes, with the red lobe being approximately twice as broad as the blue lobe. We can rule out crosstalk as the source of the asymmetry since these spectra were observed with the "anti-McMath" device, a compensator for the oblique reflection of the light path (Harvey 1985).

In both wavelength ranges, the amplitude asymmetry is positive, in accordance with observations in the optical at the corresponding μ-value (Pantellini et al. 1988). The values in the infrared are much larger, however, and do not show the same dependence on line strength as the optical data. The area asymmetry has opposite signs for the J- and H-band data. Again, our δA values are stronger and do not exhibit the same strength dependence as the optical data at the corresponding μ.

Also, the δa of all plotted lines in the J-band is larger than all the plotted δa values of the H-band lines. It is unclear whether this difference is caused completely by the larger Zeeman sensitivity of the 1.5 μm lines (Grossmann-Doerth et al. 1989) or is partly due to differences between the velocity structure of the observed regions (e.g. pores contributing more to one spectrum than the other).

The cause of the discrepancies with the visible data is not clear. The possible presence of pores in the present data and their absence in the visible data appears to be a

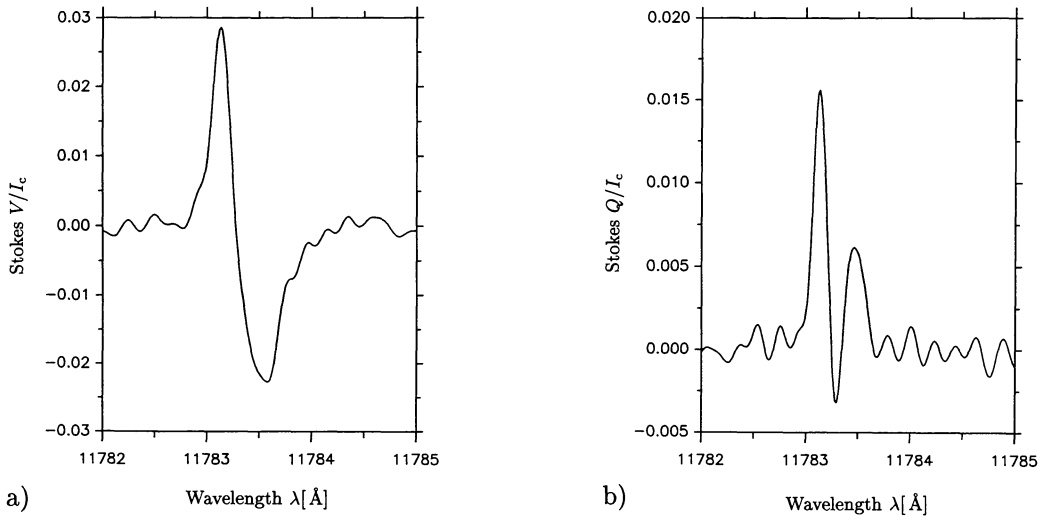

Fig. 12. Typical asymmetrical Stokes V a) and Q b) profiles in the J-band plage spectrum

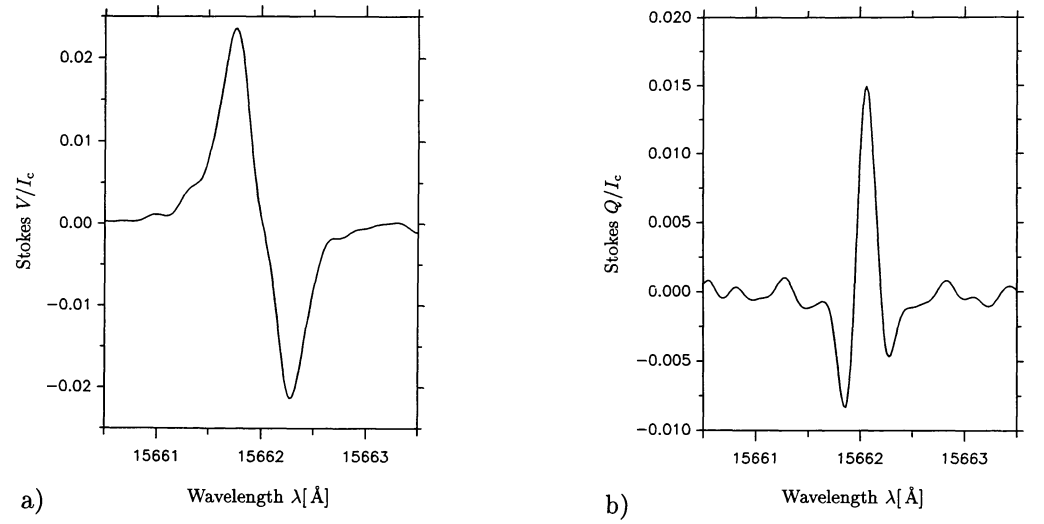

Fig. 13. Same as Fig. 12 for the H-band plage spectrum

likely candidate. It may also be that in each spectral range the lines sample the solar velocity field in a unique manner. More observations with better signal to noise ratio and sampling more areas would be necessary to obtain a better understanding of these phenomena.

11. Stokes Q asymmetry

In Fig. 14 we plot asymmetry parameters derived from the Stokes Q profiles having large amplitudes and a blending index smaller than two. The circles again represent the wavelength range between 1.1 and 1.3 μm, the crosses 1.4 to 1.7 μm. Figure 14a illustrates the σ to π asymmetry, defined as $(a_\sigma - a_\pi)/(a_\sigma + a_\pi)$, where a_σ is the sum of the unsigned amplitudes of the two σ-components and a_π is the unsigned amplitude of the π-component. Due to the large scatter of the points and the distribution of the

Table 4a. List of lines (1.1 μm−1.3 μm) with strong Q amplitude

1 Ion	2 $\lambda_\odot$ [Å]	3 Transition	4 $g_{\rm eff}^{\rm calc.}$	5 $a_b(\sigma)$	6 $a(\pi)$	7 $a_r(\sigma)$	8 blend
Al I	13123.440	$4s\ ^2S_{1/2}$—$4p\ ^2P^o_{3/2}$	1.167	4.8	1.3	2.8	0–1
Fe I	12879.778	$a\ ^3P_2$ —$z\ ^5D^o_3$	1.500	5.8	2.8	3.8	3
Si I	12031.527	$4s\ ^3P^o_2$—$4p\ ^3D_3$	1.167	4.5	1.3	2.8	2
Fe I	11884.102	$a\ ^5P_1$—$z\ ^5D^o_2$	1.000	6.2	0.6	3.2	0
Fe I	11882.859	$a\ ^5P_2$—$z\ ^5D^o_3$	1.167	5.9	0.6	2.5	0–1
Fe I	11783.289	$b\ ^3P_2$—$z\ ^3D^o_3$	1.167	5.9	0.9	2.7	0
Fe I	11689.981	$a\ ^5P_1$—$z\ ^5D^o_1$	2.000	8.5	1.7	2.1	3
Fe I	11638.232	$a\ ^5P_3$—$z\ ^5D^o_3$	1.583	7.5	1.6	4.1	3
Fe I	11607.585	$a\ ^5P_2$—$z\ ^5D^o_2$	1.667	7.8	1.6	3.6	0
Fe I	11593.618	$a\ ^5P_1$—$z\ ^5D^o_0$	2.500	10.0	4.9	5.0	2–3
Fe I	11422.333	$a\ ^5P_2$—$z\ ^5D^o_1$	2.000	9.9	4.6	5.7	0

line strengths (all of the J-band lines are strong, while the H-band lines are all comparatively weak), it is difficult to distinguish between the dependence of the σ–π

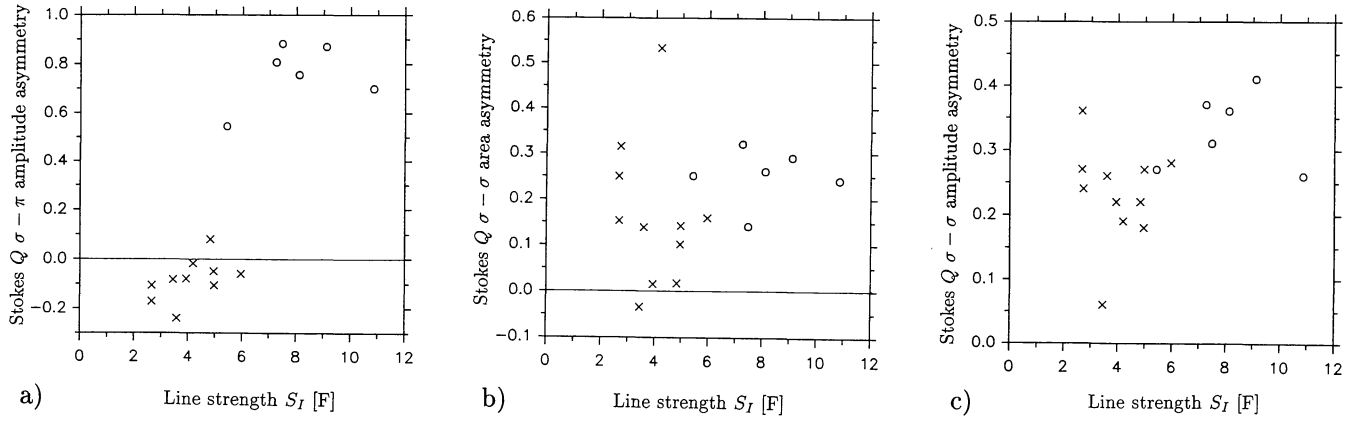

Fig. 14. Stokes Q asymmetries in the plage spectra. The symbols have the same meanings as in Fig. 11. a) $\sigma - \pi$ amplitude-asymmetry. b) $\sigma - \sigma$ area-asymmetry. c) $\sigma - \sigma$ amplitude-asymmetry

Table 4b. List of lines (1.4 μm–1.7 μm) with strong Q amplitude

1 Ion	2 $\lambda_\odot$ [Å]	3 Transition	4 $g_{\rm eff}^{\rm calc.}$	5 $a_b(\sigma)$	6 $a(\pi)$	7 $a_r(\sigma)$	8 blend
Fe I	16198.510	$e\ ^7D_2 - n\ ^7D^\circ_3$	1.500	3.5	6.7	2.2	1
Fe I	15911.318	$e\ ^5F_4 - 5p\ ^5F^\circ_3$	1.500	2.7	7.1	1.7	0–1
Fe I	15723.609	$e\ ^5D_2 - u\ ^5P^\circ_3$	1.833	4.0	7.5	2.8	0–1
Fe I	15692.772	$e\ ^7D_3 - n\ ^7D^\circ_3$	1.750	4.2	7.9	2.1	3
Fe I	15662.031	$e\ ^5F_5 - 3d^7 5p\ ^5F^\circ_4$	1.500	4.2	7.7	2.0	0–1
Fe I	15648.518	$e\ ^7D_1 - n\ ^7D^\circ_2$	3.000	2.8	9.5	1.8	0–1
Fe I	15631.960	$e\ ^7D_4 - n\ ^7D^\circ_4$	1.650	4.9	8.9	3.2	2–3
Fe I	15534.257	$e\ ^5D_1 - u\ ^5P^\circ_2$	2.000	3.5	7.7	2.0	1
Fe I	15394.718	$e\ ^5F_2 - 5p\ ^5D^\circ_2$	1.250	3.6	6.8	2.5	2
Fe I	15294.584	$e\ ^5D_5 - n\ ^7D^\circ_5$	1.550	5.8	9.3	4.6	3
Fe I	15244.988	$e\ ^5D_3 - u\ ^5F^\circ_3$	1.375	3.4	6.7	2.0	0–1
Fe I	15219.637	$e\ ^5D_3 - t\ ^5D^\circ_2$	1.500	3.8	8.5	3.3	1
Fe I	15207.545	$e\ ^7D_3 - n\ ^7D^\circ_2$	1.500	4.9	6.9	3.1	0
Fe I	15077.296	$e\ ^5D_3 - u\ ^5P^\circ_3$	1.583	3.0	7.2	1.7	3
		$a\ ^5P_3 - z\ ^7P^\circ_3$	1.792	3.0	7.2	1.7	3
Fe I	15051.765	$e\ ^7D_4 - n\ ^7D^\circ_3$	1.500	5.1	9.1	2.9	1–2
Mg I	15047.644	$4s\ ^3S_1 - 4p\ ^3P^\circ_0$	2.000	6.7	8.9	4.1	3
Mg I	15040.201	$4s\ ^3S_1 - 4p\ ^3P^\circ_1$	1.750	5.3	7.6	4.9	3
Fe I	14956.166	$4s\ ^5D_4 - t\ ^5D^\circ_3$	1.500	5.4	10.0	4.7	2
Fe I	14826.468	$e\ ^7D_5 - n\ ^7D^\circ_4$	1.500	5.4	7.6	2.8	3
Fe I	14652.917	$n\ ^7F^\circ_5 - 5d\ ^7G_6$	1.167	3.9	6.8	2.7	1

asymmetry on line strength, Zeeman splitting and differences intrinsic to the observed solar regions. The relative area and amplitude asymmetries between the red and blue σ components of Stokes Q are plotted in Fig. 14b and c. They are defined exactly as the Stokes V δA and δa, respectively. The scatter is again large in the two figures and it is not possible to see clear trends apart from the fact that almost all the values are positive. There may be a tendency for J-band lines to show larger Stokes Q $\sigma - \sigma$ asymmetry than the H-band lines. Also, the average amplitude asymmetry appears to be slightly larger than the area asymmetry. In general the Stokes Q $\sigma - \sigma$ amplitude- and area-asymmetries appear to be much stronger than their Stokes V counterparts. To our knowledge these are the first quantitative measurements of Stokes Q $\sigma - \sigma$ asymmetry.

12. Conclusions

We have surveyed the circular and linear Zeeman polarization produced in a solar active region plage and a sunspot umbra between 1.05 and 2.50 μm. Much of this spectral region has never previously been surveyed in polarized radiation. We have briefly discussed the diagnostic properties of a number of lines that are special in some way. An example is the Fe I 15648 Å line, which shows a 3 times larger Zeeman splitting than optical Zeeman–sensitive lines, but suffers from significant shortcomings in sunspot umbrae. Of particular interest for umbral investigations is the Ti I multiplet around 2.2 μm. Not only does it include an extremely sensitive Zeeman triplet ($g = 2.5$), but also has the advantage that a number of similar lines with different $g_{\rm eff}$ are present, there is no contamination of the lines by light from the quiet sun and the lines are almost completely unblended by other solar lines, even in dark parts of the umbra (where the 15648 Å line suffers from blending). The major disadvantage of the Ti I multiplet is that most of its members are significantly blended by telluric lines. We show that these blends can be removed from both the polarized and unpolarized Stokes parameters simply, accurately and reliably using observations obtained in the sunspot and in the surrounding plage (so long as the telluric atmospheric column mass is not too large at the time of the observations). It is now relatively straightforward to use these lines to investigate sunspot umbrae. Another line with unique diagnostic properties is He I 10830 Å. It is formed entirely in the upper chromosphere and is the premier diagnostic of magnetic fields at this atmospheric level. Thus, the near infrared allows us to measure magnetic fields over a large height range, from practically

the deepest observable layers (Fe I 15648 Å) to the upper chromosphere. The range over which magnetic fields can be detected in the optical is considerably smaller; the Ca II K_2 peak and the Ca I 4227 Å core are formed only in the mid chromosphere (e.g. Uitenbroek 1989; Solanki et al. 1991; Faurobert-Scholl 1992), 500–800 km below the formation level of He I 10830 Å. Combined observations of Fe I 15648 Å, Mg I 12.32 μm and He I 10830 Å should allow the field to be mapped at 3 different heights, with different physics governing its structure at each of these height.

We have systematically searched for the lines with the largest Stokes V and Q amplitudes. Such lines are particularly useful for investigations requiring high S/N ratios, such as accurate magnetic vector measurements or analyses of Stokes profile shapes, in particular line asymmetries. We have further identified a number of lines that exhibit both strong V and Q signals and thus are good candidates for magnetic vector measurements. In addition, we have considered the Stokes V and strong Q asymmetry of the lines showing strong Stokes signals. Remarkable are the lines in our J-band plage spectrum. Many of the Stokes V profiles with large amplitudes also are extremely asymmetric. In particular their red Stokes V lobe is approximately twice as wide as their blue lobe. The Stokes Q profiles are also highly asymmetric. The origin of these strong asymmetries is still unclear and deserves a more thorough analysis.

Acknowledgements. We thank C. Plymate and J. Wagner for helping with the observations and G. Ladd for transforming the FTS interferograms into spectra.

References

Abdussamatov H.I. 1971, Sol. Phys. 16, 384
Avrett E.H., Fontenla J.M., Loeser R. 1994, in Infrared Solar Phys. eds. D. Rabin, J. Jefferies, C.A. Lindsey (Kluwer, Dordrecht), IAU Symp. 154, 35
Ayres T.R. 1978, ApJ 225, 665
Ayres T.R., Testerman L., Brault J.W. 1986, ApJ 304, 542
Balthasar H., Schmidt W. 1994, A&A 290, 649
Beckers J.M. 1969, A Table of Zeeman Multiplets, AFCRL–69–0115
Biémont E., Brault J.W. 1987, Physica Scr. 35, 286
Bruls J.H.M.J., Solanki S.K. 1995, A&A 293, 240
Bruls J.H.M.J., Solanki S.K., Carlsson M., Rutten R.J. 1995, A&A 293, 225
Delbouille L., Roland G., Brault J.W., Testerman L. 1981, Photometric Atlas of the Solar Spectrum from 1850 to 10 000 cm^{-1}, NOAO, Tucson, AZ
Deming D., Boyle R.J., Jennings D.E. 1988, ApJ 333, 978
Deming D., Hewagama T., Jennings D.E., McCabe G., Wiedemann G. 1994, in Infrared Solar Phys., eds. D. Rabin, J. Jefferies, C.A. Lindsey (Kluwer, Dordrecht) IAU Symp. 154, 379
Edlén B. 1953, J. Opt. Soc. America 43, 339
Farmer C.B., Norton R.H. 1989, A High Resolution Atlas of the Infrared Spectra of the Sun and the Earth Atmosphere from Space. Vol 1. The Sun, NASA Reference Publication 1224
Faurobert-Scholl M. 1992, A&A 258, 521
Fontenla J.M., Avrett E.H., Loeser R. 1993, ApJ 406, 319
Giovanelli R.G., Hall D. 1977, Sol. Phys. 52, 211
Grevesse N., Lambert D.L., Sauval A.J. et al. 1991, A&A 242, 488
Grossmann-Doerth U., Schüssler M., Solanki S.K. 1989, A&A 221, 338
Hagyard M.J., Teuber D., West E.A. et al. 1983, Sol. Phys. 84, 13
Hall D.N.B. 1974, An Atlas of Infrared Spectra of the Solar Photosphere and of Sunspot Umbrae, Kitt Peak National Observatory, Contribution No. 556, Tucson, AZ
Harvey J.W. 1973, Sol. Phys. 28, 43
Harvey J.W. 1985, Measurements of Solar Vector Magnetic Fields, ed. M.J. Hagyard, NASA Conf. Publ. 2374, p. 109
Harvey J.W., Hall D.N.B. 1971, Solar Magnetic Fields, ed. R.F. Howard (Reidel, Dordrecht) IAU Symp. 43, 279
Harvey J.W., Hall D. 1975, BAAS 7, 459.
Henze W., Jr., Tandberg-Hanssen E., Hagyard M.J. et al. 1982, Sol. Phys. 81, 231
Hewagama T., Deming D., Jennings D.E. et al. 1993, ApJS 86, 313
Kopp G., Rabin D. 1992, Sol. Phys. 141, 253
Landi Degl'Innocenti E. 1985, Sol. Phys. 99, 1
Lee J.W., Gary D.E., Hurford G.J. 1993, Sol. Phys. 144, 45
Linsky J.L., Saar S.H. 1987, in Cool Stars, Stellar Systems and the Sun. V, eds. J.L. Linsky, R.E. Stencel (Springer, New York) 44
Litzén U. 1976, Physica Scr. 14, 165
Litzén U., Vergés J. 1976, Physica Scr. 13, 240
Livingston W., Wallace L. 1991, An Atlas of the Solar Spectrum in the Infrared from 1850 to 9000 cm^{-1} (1.1 to 5.4 μm), NSO Technical Report # 91-001, National Solar Obs., Tucson, AZ
Mathys G., Stenflo J.O. 1987, A&A 171, 368
McPherson M.R., Lin H., Kuhn J.R. 1992, Sol. Phys. 139, 255
Muglach K., Solanki S.K. 1992, A&A 263, 301
Pantellini F.G.E., Solanki S.K., Stenflo J.O. 1988, A&A 189, 263
Rabin D. 1992a, ApJ 390, L103
Rabin D. 1992b, ApJ 391, 832
Rabin D. 1994, in Infrared Solar Physics, eds. D. Rabin, J. Jefferies, C.A. Lindsey (Kluwer, Dordrecht) IAU Symp. 154, 449
Ramsauer J., Solanki S.K., Biémont E. 1995, A&AS (Paper II) in press
Rüedi I., Solanki S.K., Livingston W., Stenflo J.O. 1992, A&A 263, 323
Rüedi I., Solanki S.K., Livingston W. 1995, A&A 293, 252
Saar S.H., Linsky J.L. 1985, ApJ 299, L47
Schmidt W., Knölker M., Westendorp Plaza C. 1994, A&A 287, 229
Solanki S.K. 1994, in Infrared Solar Physics, eds. D. Rabin, J. Jefferies, C.A. Lindsey (Kluwer, Dordrecht) IAU Symp. 154, 393
Solanki S.K., Brigljević V. 1992, A&A 262, L29

Solanki S.K., Biémont E., Mürset U. 1990, A&AS 83, 307 (Paper I)
Solanki S.K., Steiner O., Uitenbroek H. 1991, A&A 250, 220
Solanki S.K., Rüedi I., Livingston W. 1992a, A&A 263, 312
Solanki S.K., Rüedi I., Livingston W. 1992b, A&A 263, 339
Solanki S.K., Walther U., Livingston W. 1993, A&A 277, 639
Solanki S.K., Livingston W., Ayres T. 1994a, Science 263, 64
Solanki S.K., Montavon C.A.P., Livingston W. 1994b, A&A 283, 221
Steiner O. 1994, in Infrared Solar Physics, eds. D. Rabin, J. Jefferies, C.A. Lindsey (Kluwer, Dordrecht) IAU Symp. 154, 407
Stenflo J.O., Solanki S.K., Harvey J.W. 1987a, A&A 171, 305
Stenflo J.O., Solanki S.K., Harvey J.W. 1987b, A&A 173, 167
Stürenburg S., Holweger H. 1990, A&A 237, 125
Uitenbroek H. 1989, A&A 213, 360
Van Ballegooijen A.A. 1984, Sol. Phys. 91, 195
Wallace L., Livingston W. 1992, An Atlas of a Dark Sunspot Umbral Spectrum from 1970 to 8640 cm^{-1} (1.16 to 5.1 μm), NSO Technical Report # 92-001, National Solar Obs., Tucson, AZ
Wallace L., Hinkle K., Livingston W. 1993, An Atlas of the Photospheric Spectrum from 8900 to 11360 cm^{-1} (7350 to 511230 Å), NSO Technical Report # 93-001, National Solar Obs., Tucson, AZ
Wallace L., Livingston W., Bernath P. 1994, An Atlas the Sunspot Spectrum from 470 to 1233 cm^{-1} (8.1 to 21 μm) and the Photospheric Spectrum from 460 to 630 cm^{-1} (16 to 22 μm), NSO Technical Report # 1994-01, National Solar Obs., Tucson, AZ
Zayer I., Solanki S.K., Stenflo J.O. 1989, A&A 211, 463